*Appl. Math. Mech. -Engl. Ed.*, **42**(9), 1297–1310 (2021)

**APPLIED MATHEMATICS AND MECHANICS (ENGLISH EDITION)**

https://doi.org/10.1007/s10483-021-2764-8

# Proper orthogonal decomposition analysis of coherent motions in a turbulent annular jet*

Y. ZHANG, M. VANIERSCHOT†

Department of Mechanical Engineering, Group T Leuven Campus,
KU Leuven, Celestijnenlaan 300, Leuven B-3001, Belgium

(Received Apr. 12, 2021 / Revised Jun. 11, 2021)

**Abstract** A three-dimensional incompressible annular jet is simulated by the large eddy simulation (LES) method at a Reynolds number $Re = 8\,500$. The time-averaged velocity field shows an asymmetric wake behind the central bluff-body although the flow geometry is symmetric. The proper orthogonal decomposition (POD) analysis of the velocity fluctuation vectors is conducted to study the flow dynamics of the wake flow. The distribution of turbulent kinetic energy across the three-dimensional POD modes shows that the first four eigenmodes each capture more than 1% of the turbulent kinetic energy, and hence their impact on the wake dynamics is studied. The results demonstrate that the asymmetric mean flow in the near-field of the annular jet is related to the first two POD modes which correspond to a radial shift of the stagnation point. The modes 3 and 4 involve the stretching or squeezing effects of the recirculation region in the radial direction. In addition, the spatial structure of these four POD eigenmodes also shows the counter-rotating vortices in the streamwise direction downstream of the flow reversal region.

**Key words** coherent structure, proper orthogonal decomposition (POD), turbulent annular jet, large eddy simulation (LES)

**Chinese Library Classification** O358
**2010 Mathematics Subject Classification** 76F10

## 1 Introduction

An annular jet, which is regarded as the limiting case of a coaxial jet[1], is utilized widely in combustion devices[2–3]. Early studies showed that annular jets share the similarity properties (such as expansion, decay, and mean axial velocity profiles) of those found in turbulent round jets in the far-field region[4–6]. Apart from the jet characteristics, the flow field of an annular jet also features a wake flow near the nozzle. Due to the existence of a central obstacle, flow separation occurs, and a recirculation region is developed behind it, which is served as a way to enhancing a fuel-air mixing rate and reducing pollutant emission in combustion systems. Also, the central bluff-body can have a function as an injector, from which fuel can be injected

* Citation: ZHANG, Y. and VANIERSCHOT, M. Proper orthogonal decomposition analysis of coherent motions in a turbulent annular jet. *Applied Mathematics and Mechanics* (*English Edition*), **42**(9), 1297–1310 (2021) https://doi.org/10.1007/s10483-021-2764-8

† Corresponding author, E-mail: maarten.vanierschot@kuleuven.be

Project supported by China Scholarship Council (No. 201706890016)

axially or radially[7]. In addition, two shear layers originating from the annular orifice exist in the near-field. The outer shear layer is between an ambient medium and a jet, and the inner shear layer is between a recirculation zone and a jet. These two shear layers meet and interact with each other downstream of the reversal flow region[8].

Although the flow has both a symmetric geometry and symmetric boundary conditions, the investigations on turbulent annular jets have shown that spontaneous break of symmetry of the time-averaged flow field could appear[9–14]. This type of asymmetry is observed in laminar annular jets as well, if the Reynolds number is above a certain threshold value, which is around 150 for the geometry used in this study[15]. In turbulent regimes, this asymmetry is illustrated by a low-frequency oscillating vortex shedding from the buff-body that is convected to the end of the recirculation zone, creating a shift of the stagnation point in the radial direction[8, 9, 11, 16]. On the other hand, in the laminar regime, Del Taglia et al.[13] found that the occurrence of this flow asymmetry is influenced by the jet blockage ratio and the Reynolds number, which can be integrated as a state parameter. Similar kinds of asymmetric flow patterns were also observed in other flow configurations, such as in turbulent wakes past blunt bodies[17–18].

Several investigations have been conducted to address the asymmetric mean wake in turbulent annular jets. Patte-Rouland et al.[8] applied the proper orthogonal decomposition (POD) to the particle image velocimetry (PIV) velocity fields and showed that the asymmetric flow is related to the first two POD modes. It should also be noted that the POD analysis is not applied on the fluctuating velocity part but on the instantaneous fields, which means that the first POD mode denotes the mean flow. However, their PIV velocity fields are two-dimensional, and no temporal dynamics is obtained owing to the relative low sampling frequency. Vanierschot and Van den Bulck[11] investigated the precession of the central toroidal vortex behind the central bluff-body using the phase averaging method, which treats the coherent fluctuations in the flow field as a whole. The symmetry breaking and vortex precession in low-swirling annular jets were studied by Vanierschot et al.[12] with PIV and POD techniques, showing that the motion of the asymmetric wake is random in time. The drawback of their study is that the measured PIV velocity vectors were two-dimensional as well. The first experimental study to reveal the three-dimensional structure of the wake was done by Vanierschot et al.[16]. Using tomographic PIV measurements, they found several asymmetric vortical structures which were shed from the inner shear layer towards the stagnation point.

This study aims to reveal the connection between the asymmetric mean flow field and the turbulent coherent motions in an annular jet. First, the flow is simulated by the large eddy simulation (LES) method. Then, the snapshot POD technique is adopted to capture the most energetic coherent structures in the fluctuating flow. The main concerns here are the spatial structures of the low-frequency coherent motions and their relationship with the flow dynamics, especially on the wake or recirculation region behind the central bluff-body. To the authors' knowledge, a three-dimensional POD analysis of detailed LES data has not been conducted yet. The remainder of this paper is organized as follows. The numerical method is briefly introduced in Section 2. Section 3 presents the asymmetric time-averaged flow field. The POD analysis of the velocity fields is given in Section 4. Finally, we summarize our findings and present the conclusions in Section 5.

## 2 Numerical method

The governing equations for the concerned flow are the filtered three-dimensional incompressible Navier-Stokes equations for the Newtonian fluids,

$$\frac{\partial \overline{u}_i}{\partial t} + \frac{\partial (\overline{u}_i \overline{u}_j)}{\partial x_j} = -\frac{\partial \overline{p}}{\partial x_i} + \nu \frac{\partial^2 \overline{u}_i}{\partial x_j \partial x_j} - \frac{\partial \tau_{ij}}{\partial x_j}, \tag{1}$$

$$\frac{\partial \overline{u}_i}{\partial x_i} = 0. \tag{2}$$

Here, $\overline{u}_i$ are the resolved velocities, $\overline{p}$ is the filtered kinematic pressure, $t$ is time, $x_i$ are spatial coordinates, and $\nu$ is the kinematic viscosity of the fluid. The subgrid-scale stress tensor $\tau_{ij} = \overline{u_i u_j} - \overline{u}_i \overline{u}_j$ in the above formulation is modeled by the localized dynamic $k$ model introduced by Kim and Menon[19–20]. Recently, we have used the same numerical approach to simulate the turbulent annular swirling jet flow in a similar configuration to identify the helical vortex cores in the flow field[21]. It was found that the numerical results were in line with experimental measurements, validating the approach. The only difference in this work is that, for a zero swirl intensity annular jet, there is no tangential injection of fluid in the swirl generator, as depicted in Fig. 1(a). The annular jet is generated by a fluid (water with a viscosity $\nu = 1.005 \times 10^{-6}$ m$^2$/s) flowing through a swirl generator with twelve fixed and movable blocks, and then guided into the passage between two coaxial cylinders. The configuration of the annular tube near the jet orifice is shown in Fig. 1(b). The diameters of the inner and outer cylinders are $D_\mathrm{i} = 18$ mm and $D_\mathrm{o} = 27$ mm, respectively. The Reynolds number $Re = u_0 D_\mathrm{h}/\nu$ is around 8 500, where $u_0 = 0.95$ m/s is the mean axial velocity at the jet nozzle, and $D_\mathrm{h} = 9$ mm is the hydraulic diameter of the annular flow passage.

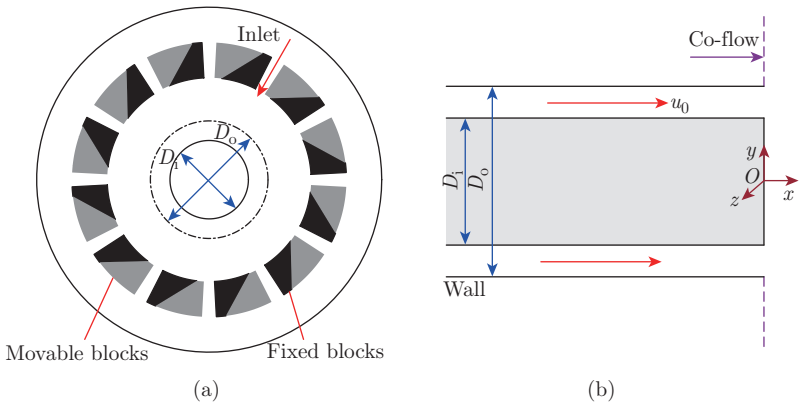


**Fig. 1** (a) The schematic layout of the swirl generator and (b) the configuration of the annular pipe close to the jet nozzle (color online)

The governing equations are solved by the open-source C++ library OpenFOAM based on the finite volume method. The temporal discretization scheme is second-order implicit backward. For the spatial derivative terms, the convective term is discretized by a second-order upwind scheme, whereas the diffusive term is approximated by a second-order central difference scheme. The computational grid is hexahedrally structured and nonuniform and has a total number of around 10.5 million cells. There are 384 control volumes in the azimuthal direction and 356 cells in the main flow direction from the inlet to the outlet. The finest grid spacing is situated at the jet orifice with $\Delta x = D_\mathrm{o}/600$ in the axial direction and $\Delta r = D_\mathrm{o}/1\ 200$ in the radial direction. The time step is fixed at $8 \times 10^{-6}$ s to meet the Courant-Friedrichs-Lewy condition, and the maximum Courant number is less than 0.55 during the simulation. The detailed information about the numerical method and its validation can be found in our previous work[21].

## 3 Asymmetric mean flow field

Different views of the time-averaged reversal flow area obtained during 300 dimensionless time units (calculated as $tu_0/D_\mathrm{o}$) are presented in Figs. 2(a) and 2(b). From the figures, we

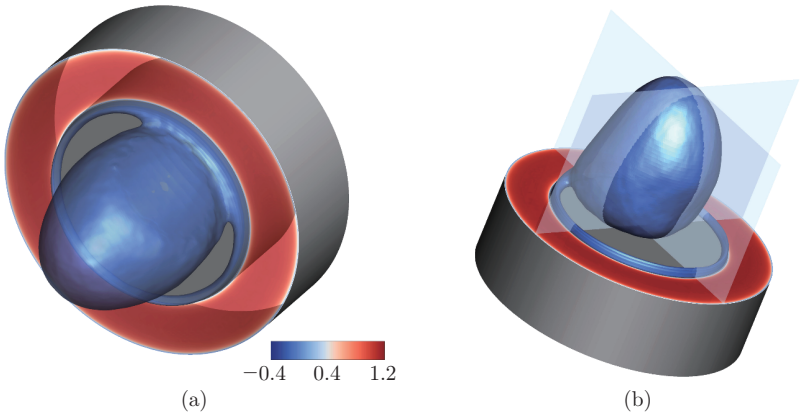


**Fig. 2** Different views of the backflow region shown by the iso-surface of the normalized mean axial velocity $\langle\overline{u}\rangle/u_0 = 0$ behind the central bluff-body, (a) the zero axial velocity iso-surface, (b) the position of the symmetric and asymmetric planes, where the slices in (b) indicate the defined "asymmetric" and "symmetric" planes (color online)

can see that the recirculation zone behind the inner cylinder is asymmetric although the flow configuration has an axisymmetric geometry. It is worth mentioning that the backflow region is precessing gradually around the jet central axis as the averaging time interval increases, which means that it contains very low frequency dynamics. Depending on the shape of the recirculation zone, both an "asymmetric" plane and a "symmetric" plane can be defined, similar to the study of Vanierschot et al.[16], and both planes are perpendicular to each other, as indicated by the slices in Fig. 2(b). Here, the "asymmetric" plane can be obtained by the cross-section cutting through the axis of symmetry and the stagnation point, whereas the "symmetric" plane is orthogonal to it[10, 16]. Figures 3(a) and 3(b) show the corresponding time-averaged axial velocity field $\langle\overline{u}\rangle/u_0$ and velocity vectors in these two planes, where the radius $r$ is calculated as $r = \sqrt{y^2 + z^2}$. The stagnation point that indicates the end of the recirculation region is located at $x/D_\mathrm{o} = 0.55$. As shown in the figures, the reversal flow region is not parallel to the jet central axis in the asymmetric plane, and it is almost parallel to the jet center axis in the symmetric plane. These results agree well with the findings reported by Ryzhenkov et al.[10] and Vanierschot et al.[16]. Furthermore, the normalized normal Reynolds stress $\langle\overline{u'u'}\rangle/u_0^2$ in these two planes is expressed in Figs. 3(c) and 3(d). The figures show that large velocity fluctuations exist in the inner and outer shear layer regions owing to turbulent mixing. The largest normal Reynolds stress is located in the inner shear layer in the asymmetric plane, which is caused by the highly dynamic properties of the reversal region or oscillations of the stagnation point[8]. This phenomenon was also observed in a laminar annular jet at $Re = 180$ by Ogus et al.[14].

## 4 POD modes

POD looks for spatial base functions that capture the most energetic components of a dynamical system[22]. Suppose that $N$ snapshots of the three-dimensional velocity field $\boldsymbol{u}(\boldsymbol{x}, t)$ are recorded during the numerical simulation, and POD decomposes the fluctuating velocity $\boldsymbol{u}'(\boldsymbol{x}, t)$ into a set of spatial modes $\boldsymbol{\psi}_i(\boldsymbol{x})$ with temporal coefficients $\boldsymbol{a}_i(t)$,

$$\boldsymbol{u}(\boldsymbol{x}, t) = \langle\boldsymbol{u}(\boldsymbol{x}, t)\rangle + \sum_{i=1}^{N} \boldsymbol{a}_i(t)\boldsymbol{\psi}_i(\boldsymbol{x}), \tag{3}$$

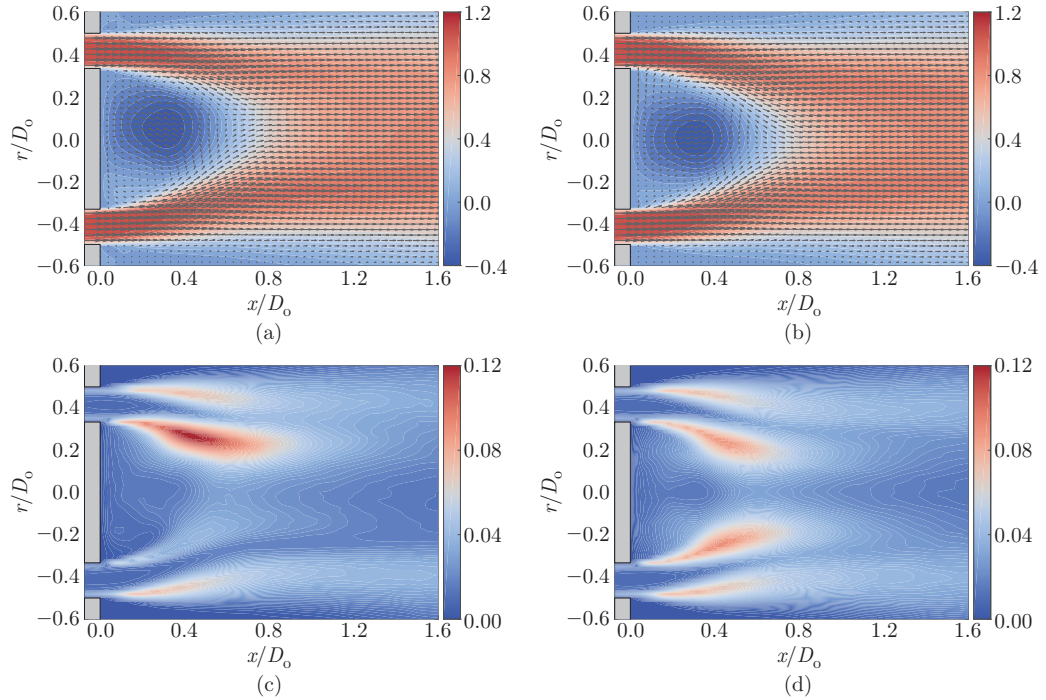


**Fig. 3** The normalized mean axial velocity $\langle\overline{u}\rangle/u_0$ in the (a) asymmetric and (b) symmetric planes, and the normalized normal Reynolds stress $\langle\overline{u'u'}\rangle/u_0^2$ in the (c) asymmetric and (d) symmetric planes (color online)

by separating the independent variables $\boldsymbol{x}$ and $t$. In this work, the snapshot POD approach of Sirovich was adopted[23–24]. The mode amplitude $\boldsymbol{a}_i(t)$ is obtained from the eigenvectors of the auto-correlation matrix $C_{i,j} = \frac{1}{N}[\boldsymbol{u}'(\boldsymbol{x}, t_i)]^{\mathrm{T}}[\boldsymbol{u}'(\boldsymbol{x}, t_j)]$,

$$\boldsymbol{C}\boldsymbol{a}_i = \lambda_i \boldsymbol{a}_i \quad \text{with} \quad \lambda_1 \geqslant \lambda_2 \geqslant \cdots \geqslant \lambda_N \geqslant 0. \tag{4}$$

Here, the eigenvalues $\lambda_i$ stand for the energy contained by each spatial mode. The eigenfunctions $\boldsymbol{\psi}_i(\boldsymbol{x})$ are calculated by projection of the snapshots onto the temporal coefficients $a_i(t)$,

$$\boldsymbol{\psi}_i(\boldsymbol{x}) = \frac{1}{N\lambda_i}\sum_{j=1}^{N} \boldsymbol{a}_i(t_j)\boldsymbol{u}'(\boldsymbol{x}, t_j). \tag{5}$$

The asymmetric recirculation zone discussed in Section 3 originates from random perturbations which are shedding from the central cylinder and are convected downstream[8–9]. Although the asymmetric time-averaged statistics of the velocity fields are observed, an appropriate choice of the time averaging interval could provide an axisymmetric flow field. Figures 4(a) and 4(b) give the averaged streamwise velocity in an axial plane and in a cross-section (at $x/D_o = 0.4$), which is calculated from 500 instantaneous flow fields ($N = 500$). The time interval between two successive snapshots is 0.024 s, corresponding to a total sampling time of 12 s. It is seen that the axial velocity field is almost symmetric about the jet central axis in Figs. 4(a) and 4(b), i.e., the averaged flow field contains an axisymmetric recirculation region. Therefore, these 500 snapshots are used in the POD analysis. Figures 5(a) and 5(b) respectively provide the distributions of turbulent kinetic energy across the three-dimensional POD modes and the accumulated energy distributions. In Fig. 5(a), we can see that the first four POD modes all

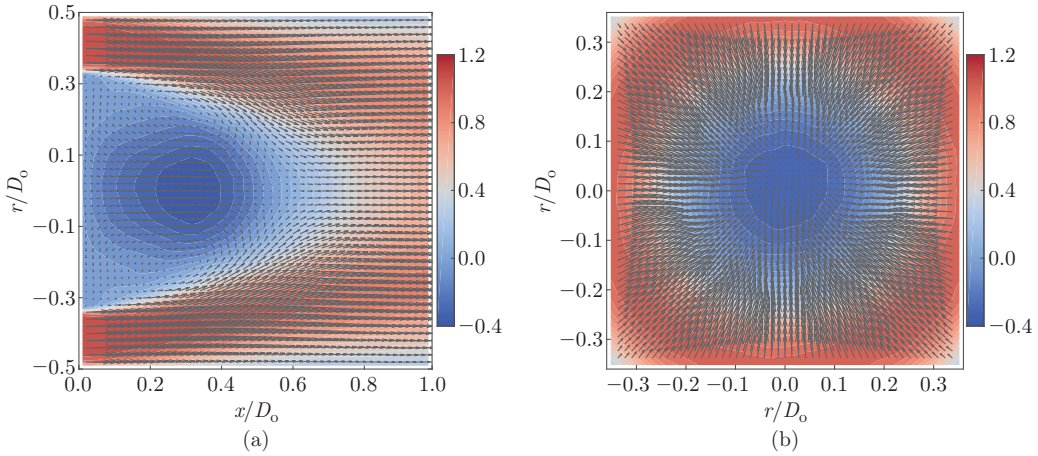


**Fig. 4** The averaged axial velocity $\langle \overline{u} \rangle$ calculated from 500 snapshots in the (a) axial and (b) cross-sectional slices, normalized by $u_0$, where the arrows in the figures represent the velocity vectors in the plane (color online)

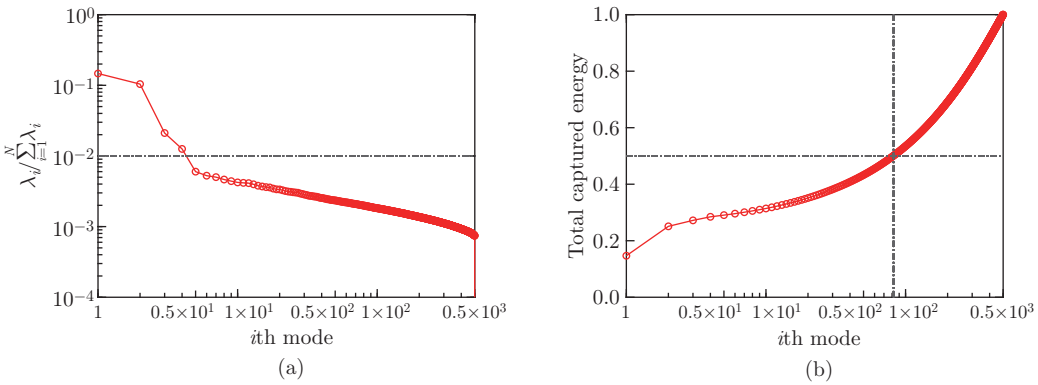


**Fig. 5** (a) The energy content of the $i$th POD mode in log-log scale and (b) the accumulated energy captured by the first $i$ POD modes in semi-log scale (color online)

have a turbulent kinetic energy content larger than 1%. In detail, the modes 1 and 2 account for 14.7% and 10.4%, respectively, while the modes 3 and 4 capture 2.1% and 1.3% of the total turbulent kinetic energy. In contrast, the remaining POD modes are weaker as each of them represents less than 1% of the total turbulent kinetic energy. If the Reynolds number is increased, the first four modes would capture less kinetic energy. The reason is that more small-scale turbulent structures appear in the flow field with increasing the Reynolds number, and these fine scale structures also have a contribution to the energy content, which means that the relative contribution of the large scale structures decreases. The dash-dotted line in Fig. 5(b) indicates that the first 82 POD modes reach more than 50% of the total energy. We will illustrate the first four eigenmodes in the following contents, as no noticeable spatial structures can be found in the other ones.

The first POD modes in an axial plane and a cross-section (at $x/D_o = 0.6$) are plotted in Figs. 6(a) and 6(b), respectively. In the axial plane, two vortices can be identified between the inner and outer mixing layers. In addition, a strong vortex is located immediately behind the central bluff-body, which leads to a radial movement of the fluid in the recirculation region.

This effect is responsible for the shift of the stagnation point as well. The results discussed here are in line with the two-dimensional PIV measurements by Patte-Rouland et al.[8] and by Vanierschot et al.[12, 25]. Moreover, the velocity vectors of the first spatial mode display a pair of counter-rotating vortices in the streamwise direction, as shown in Fig. 6(b). The structure of the second POD mode is very similar to the first one, with an angular difference of $\pi/2$ in the azimuthal direction, as presented in Figs. 6(c) and 6(d). As a consequence, the two-dimensional POD analyses conducted in previous studies[8, 12, 25] cannot depict these two modes accurately. The amplitudes of the first two spatial modes as a function of time are plotted in Fig. 7(a). It can be seen that, although the temporal coefficients exhibit small scale fluctuations in time, the curves show a general periodic trend. The normalized cross-correlation coefficient $c_{12}$ of $a_1$ and $a_2$ is given in Fig. 7(b), where $c_{ij}(\Delta t) = \langle a_i(t + \Delta t)a_j(t)\rangle$. The main features of the correlation coefficient are the maxima and minima of the curves, showing the periodicity of the motion of the first two modes in the near-field of the annular jet. The positive and negative peaks correspond to a period of around 12 s, demonstrating that the coherent motions are in the low-frequency regime. From the results above, it can be concluded that the first two POD modes have a similar spatial structure and amplitude and hence form a mode pair. The motion of this

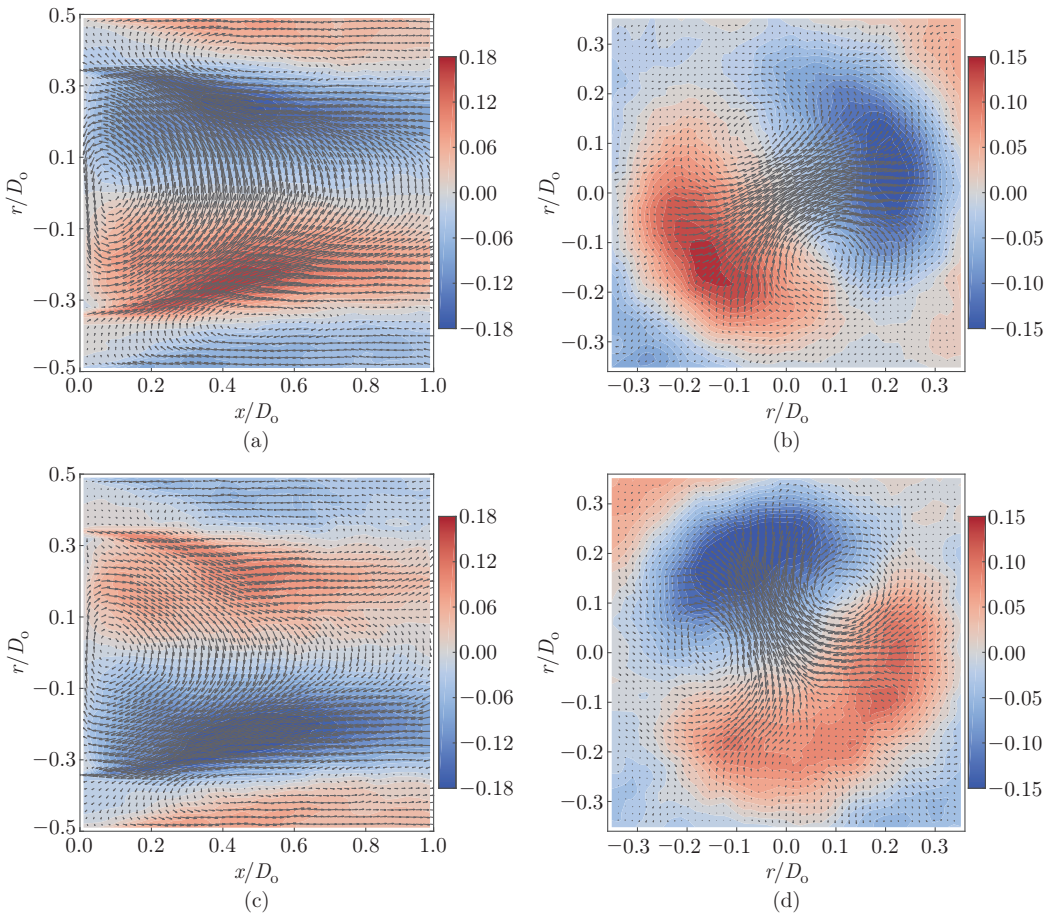


**Fig. 6** Streamwise components of $100 \times \boldsymbol{\psi}_1(\boldsymbol{x})/u_0$ in the (a) axial and (b) cross-sectional slices, and streamwise components of $100 \times \boldsymbol{\psi}_2(\boldsymbol{x})/u_0$ in the (c) axial and (d) cross-sectional slices, where the arrows in the figures represent the velocity vectors in the plane (color online)

pair accounts for 25.1% of the total turbulent kinetic energy. It should be noted that the period obtained from the cross-correlation coefficient may only describe the periodic motion roughly, since the POD analysis only includes sampled data during about one period. More numerical data however would need much more simulation time. To study the dynamical structures in the flow of smaller frequencies, a wavelet analysis of the mode amplitudes $a_1$ and $a_2$ is done. The results are plotted in Figs. 7(c) and 7(d), respectively. The figures show that the temporal coefficients have low-frequency fluctuating components from 0.28 Hz to 8.81 Hz, corresponding to a Strouhal number $St = fD_\mathrm{h}/u_0$ between $2.7\times10^{-3}$ and 0.083. This dimensionless frequency range is much lower than the one associated with inner shear layer instabilities, which is in the order of 0.15–0.3[6, 16].

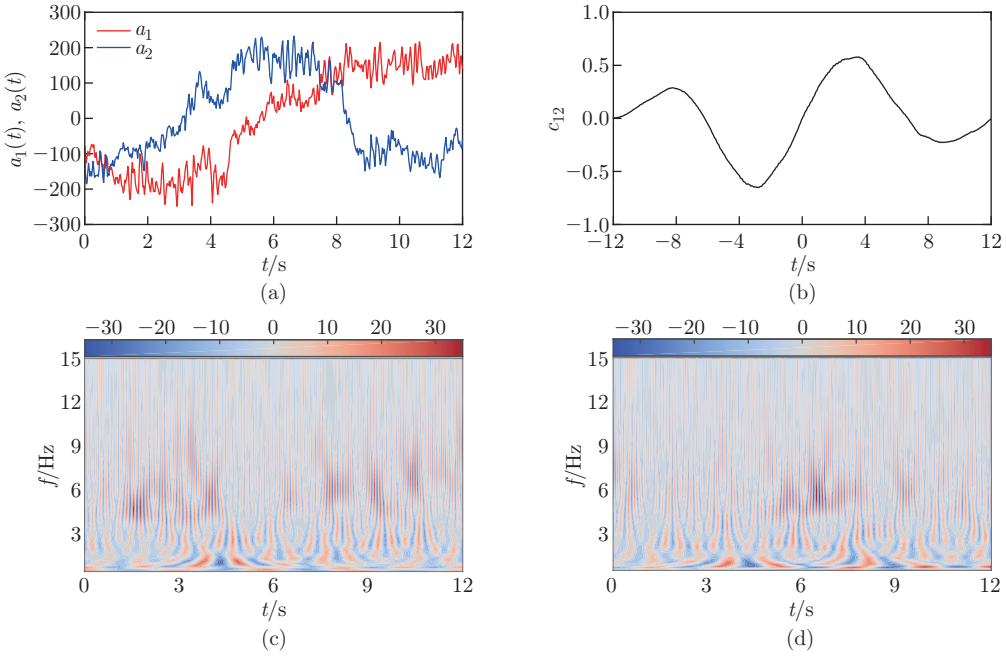


**Fig. 7** (a) Time evolution of the first and second POD mode amplitudes, (b) their cross-correlation coefficient, and the wavelet analysis of the (c) first and (d) second POD mode amplitudes (color online)

Figures 8(a) and 8(b) present the third POD mode in the axial and cross-sectional planes (at $x/D_\mathrm{o} = 0.6$), respectively. As shown in the figure, the mode 3 is symmetric about the jet central axis. The largest magnitude of the velocity is located in the area close to the end of the reversal flow region. As discussed later, this mode represents the stretching and squeezing effects in the radial direction of the reversal flow in its end region. In other words, it depicts the opening and closing of the annular jet. Furthermore, two pairs of counter-rotating vortices result from this mode in the streamwise direction. Similar to the first mode pair, the fourth POD mode has a similar structure as the third one, with an angle difference of $\pi/4$ in the azimuthal direction, as presented in Figs. 8(c) and 8(d). Figure 9(a) plots the time evolution of the amplitudes of the modes 3 and 4, and their cross-correlation coefficient $c_{34}$ is given in Fig. 9(b). The positive and negative peaks in the curve show that this mode pair has a period of about 6 s, i.e., its period is half the precession period of the first mode pair, which is in line with the result obtained by Vanierschot et al.[25]. This mode pair represents 3.4% of the total turbulent kinetic energy. Figures 9(c) and 9(d) give the wavelet analysis of the mode

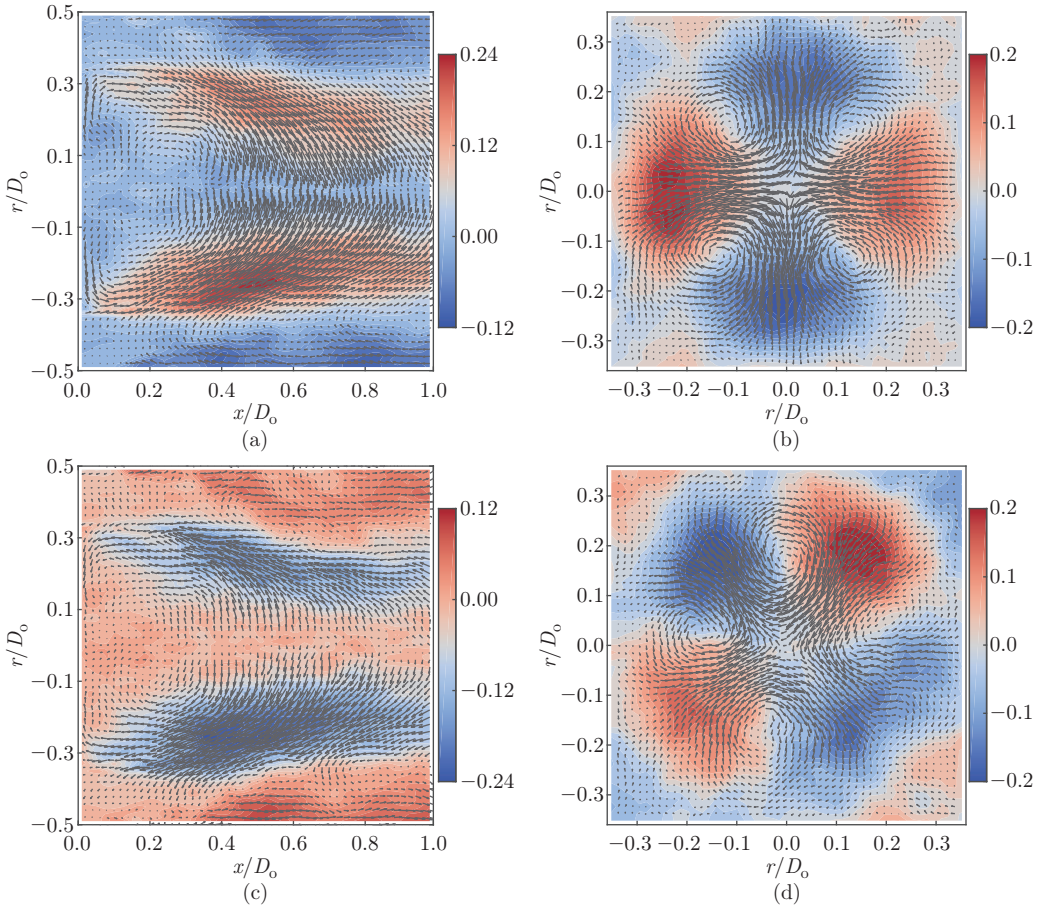


**Fig. 8** Streamwise components of $100 \times \boldsymbol{\psi}_3(\boldsymbol{x})/u_0$ in the (a) axial and (b) cross-sectional slices, and streamwise components of $100 \times \boldsymbol{\psi}_4(\boldsymbol{x})/u_0$ in the (c) axial and (d) cross-sectional slices, where the arrows in the figures represent the velocity fields in the plane (color online)

amplitudes $a_3$ and $a_4$, respectively. The wavelet coefficients again reveal that large time scale fluctuation components exist in the flow field.

To reveal the relationship between the POD mode pairs and the asymmetric flow reversal, the velocity field is reconstructed with selected spatial modes as

$$\boldsymbol{u}(\boldsymbol{x}, t) = \langle \boldsymbol{u}(\boldsymbol{x}, t) \rangle + \sum_k a_k(t) \boldsymbol{\psi}_k(\boldsymbol{x}). \tag{6}$$

Figures 10(a)–10(d) display the positive and negative iso-surfaces of $\boldsymbol{\psi}_k(\boldsymbol{x})$ for the first four POD modes, respectively. The axial component of those eigenmodes presents a pulsatile motion along the streamwise direction. Also, it verifies the harmonic relation between the spatial modes in the first and second mode pairs. The recirculation regions in the wake flow reconstructed by the first mode pair with maximum and minimum temporal coefficients are given in Figs. 10(e) and 10(f), respectively. The shape of the reversal flow zone in Figs. 10(e) and 10(f) is similar to the one shown in Fig. 2. The velocity fields reconstructed by the first mode pair in the asymmetric and symmetric planes, defined in Fig. 2(b), are illustrated in Figs. 11(a) and 11(b), respectively. It shows two vortices that have different sizes in the asymmetric plane, and two vortices that almost have the same size in the symmetric plane. The flow patterns shown in

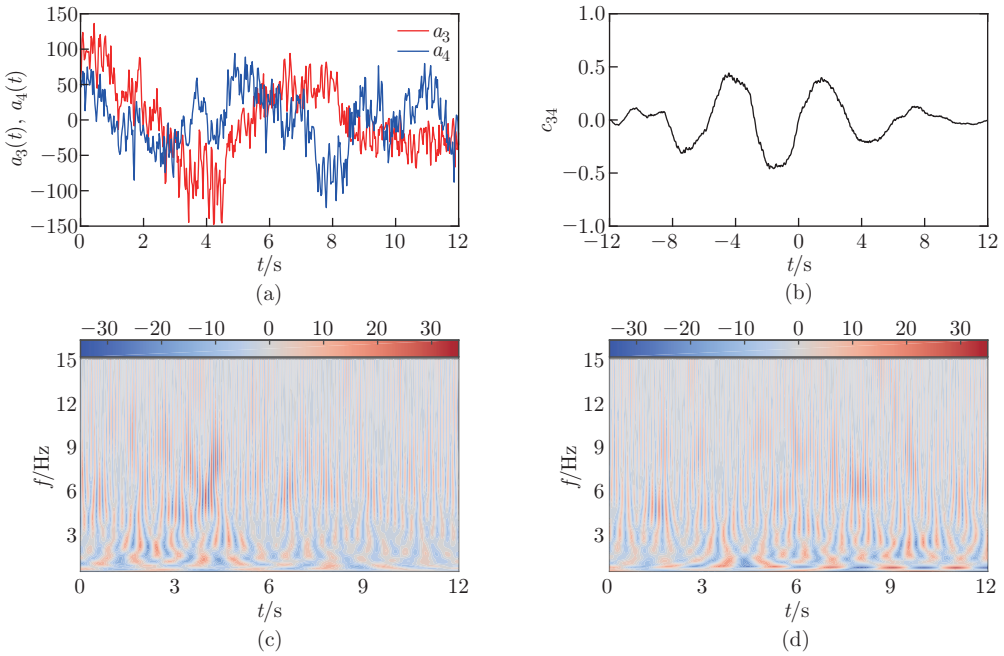


**Fig. 9** (a) Time evolution of the third and fourth POD mode amplitudes, (b) their cross-correlation coefficient, and the wavelet analysis of the (c) third and (d) fourth POD mode amplitudes (color online)

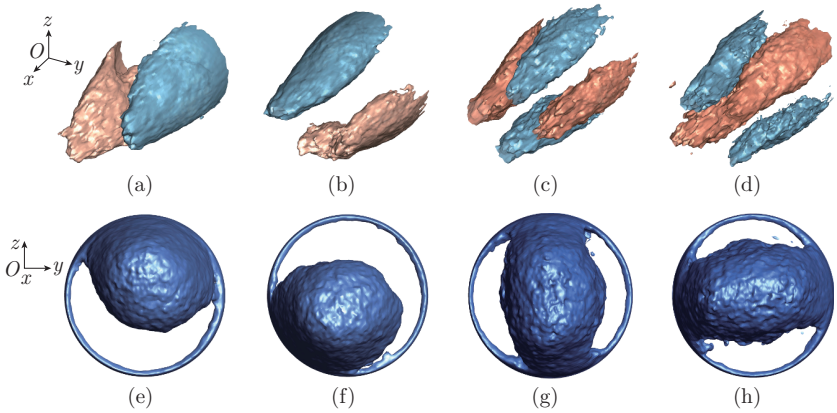


**Fig. 10** The positive (red) and negative (blue) iso-surfaces of the first four POD modes' axial component $100 \times \boldsymbol{\psi}_{k,x}(\boldsymbol{x})/u_0 = \pm 0.08$ shown in (a)–(d), respectively, and the recirculation region reconstructed by the first mode pair with (e) maximum and (f) minimum temporal coefficients, and by the second mode pair with (g) maximum and (h) minimum temporal coefficients (color online)

Fig. 11 agree with those presented in Figs. 3(a) and 3(b). Therefore, the first two POD modes are responsible for the asymmetric flow field in the wake and the associated motion of the stagnation point. The recirculation regions in the wake flow reconstructed by the second mode pair with maximum and minimum temporal coefficients are given in Figs. 10(g) and 10(h), respectively. From the figures, we can see that the reversal flow is symmetric in the two slices

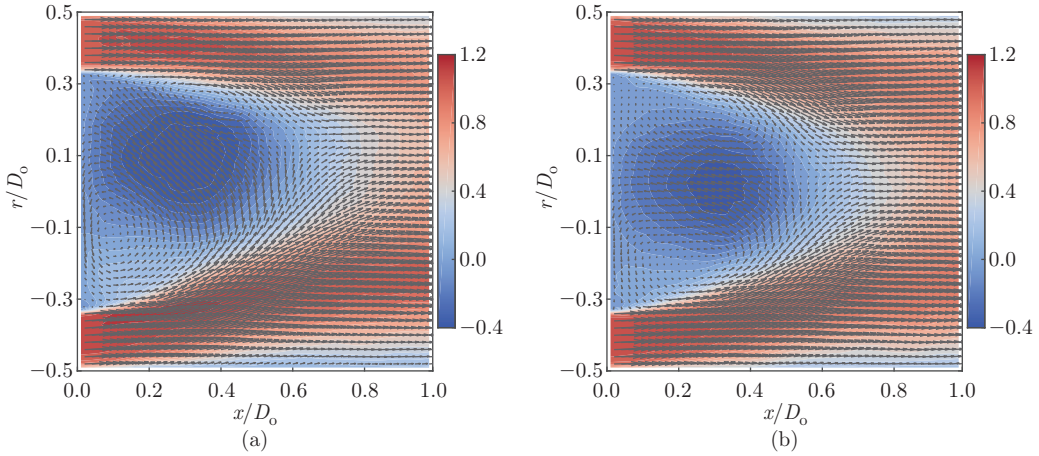


**Fig. 11** Velocity fields reconstructed by the first and second POD modes in the (a) asymmetric and (b) symmetric planes (color online)

defined in Fig. 2(b), i.e., it has two symmetric planes. The velocity fields reconstructed by the modes 3 and 4 in these two slices are respectively given in Figs. 12(a) and 12(b). The velocity vectors in both slices show two vortices between the backflow region and the inner shear layer. However, the vortices in Fig. 12(a) are smaller compared with those in Fig. 12(b). The reason is that the recirculation zone is stretched in the radial direction in Fig. 12(a), whereas it is squeezed in the radial direction in Fig. 12(b), as depicted in Figs. 10(g) and 10(h). Moreover, Figs. 10(e)–10(h) show that the recirculation regions reconstructed with maximum and minimum mode amplitudes have a phase difference of $\pi$ in the azimuthal direction, although it is not exactly the case for the first mode pair owing to the fluctuation of the temporal coefficient. This behavior confirms that the reversal flow zone is precessing around the jet central axis, as mentioned in Section 3. Figures 13(a) and 13(b) respectively describe the axial velocity field reconstructed by the first and second mode pairs at $x/D_o = 0.4$. The flow field reconstructed by the first two POD modes shows a counter-rotating vortex pair in the streamwise direction. In contrast, the

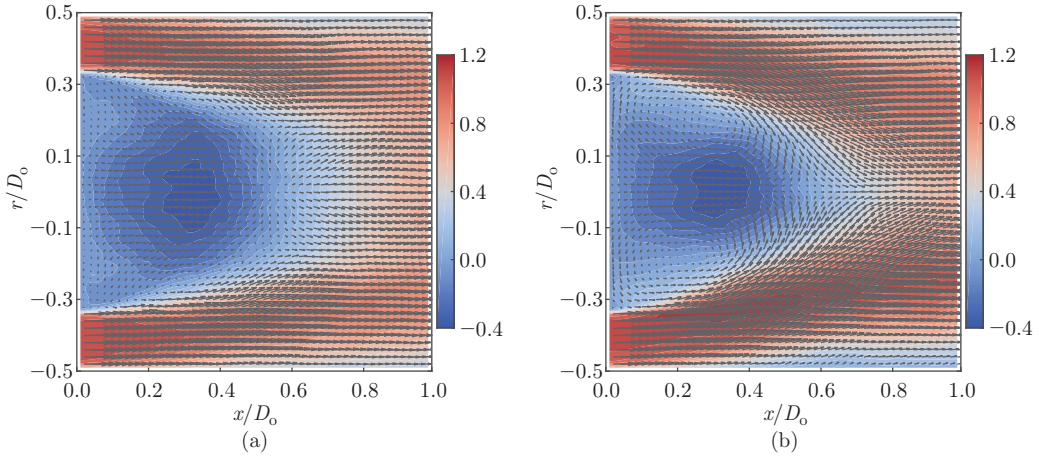


**Fig. 12** Velocity fields reconstructed by the (a) third and (b) fourth POD modes in the two symmetric planes (color online)

flow fields reconstructed by the modes 3 and 4 display two pairs of counter-rotating vortices in the main flow direction, but they are weaker as the second mode pair captures lower turbulent kinetic energy. The counter-rotating streamwise vortices were detected by the phase averaging method applied to the wake in an annular jet[11], and they were also observed in a laminar annular jet flow[14].

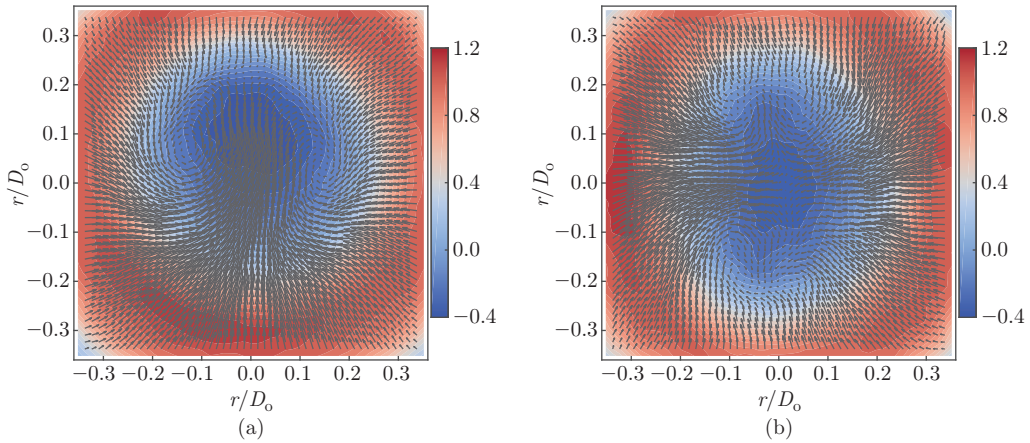


**Fig. 13** The streamwise vortices in the flow field reconstructed by (a) the first and second POD modes, and by (b) the third and fourth POD modes (color online)

## 5 Conclusions

In summary, we present the flow dynamics of the wake in a turbulent annular jet at a Reynolds number $Re = 8\,500$. It is found that the time-averaged velocity field is asymmetric although the flow has a symmetric geometry and boundary conditions. The POD analysis of the fluctuating velocity field shows that the influence of the first four eigenmodes on the mean flow cannot be neglected. The first two spatial modes account for 25.1% of the total turbulent kinetic energy, while the modes 3 and 4 only represent 3.4% of the total energy. The first POD mode pair leads to the radial movement of the fluid in the recirculation region. It corresponds to the shift of stagnation point in the radial direction and is responsible for the asymmetric time-averaged reversal flow region. In contrast, the second mode pair has stretching and squeezing effects on the recirculation region in the radial direction. The flow fields reconstructed by these four spatial modes demonstrate that the recirculation zone precesses around the jet central line at a very low frequency, corresponding to a Strouhal number $St$ less than 0.001. Moreover, the flow fields reconstructed by those two POD mode pairs also present counter-rotating vortices in the streamwise direction downstream of the reversal flow region.

**Acknowledgements** The simulation was carried out on the Tier-2 cluster of the Flemish Supercomputer Center.

## References


[1] CHIGIER, N. A. and BEEŔ, J. M. The flow region near the nozzle in double concentric jets. *Journal of Basic Engineering*, **86**(4), 797–804 (1964)

[2] CANDEL, S., DUROX, D., SCHULLER, T., BOURGOUIN, J. F., and MOECK, J. P. Dynamics of swirling flames. *Annual Review of Fluid Mechanics*, **46**, 147–173 (2014)

[3] ZHANG, Y. and VANIERSCHOT, M. Modeling capabilities of unsteady RANS for the simulation of turbulent swirling flow in an annular bluff-body combustor geometry. *Applied Mathematical Modelling*, **89**, 1140–1154 (2021)

[4] CHAN, W. T. and KO, N. W. M. Coherent structures in the outer mixing region of annular jets. *Journal of Fluid Mechanics*, **89**(3), 515–533 (1978)

[5] KO, N. W. M. and CHAN, W. T. Similarity in the initial region of annular jets: three configurations. *Journal of Fluid Mechanics*, **84**(4), 641–656 (1978)

[6] KO, N. W. M. and CHAN, W. T. The inner regions of annular jets. *Journal of Fluid Mechanics*, **93**(3), 549–584 (1979)

[7] VANIERSCHOT, M., PERSOONS, T., and VAN DEN BULCK, E. A new method for annular jet control based on cross-flow injection. *Physics of Fluids*, **21**(2), 025103 (2009)

[8] PATTE-ROULAND, B., LALIZEL, G., MOREAU, J., and ROULAND, E. Flow analysis of an annular jet by particle image velocimetry and proper orthogonal decomposition. *Measurement Science and Technology*, **12**(9), 1404–1412 (2001)

[9] DEL TAGLIA, C., BLUM, L., GASS, J., VENTIKOS, Y., and POULIKAKOS, D. Numerical and experimental investigation of an annular jet flow with large blockage. *Journal of Fluids Engineering*, **126**(3), 375–384 (2004)

[10] RYZHENKOV, V. O., ABDURAKIPOV, S. S., and MULLYADZHANOV, R. I. The asymmetry of the recirculation zone of the annular jet with different diameter ratio. *Journal of Physics*: *Conference Series*, **1382**, 012035 (2019)

[11] VANIERSCHOT, M. and VAN DEN BULCK, E. Experimental study of low precessing frequencies in the wake of a turbulent annular jet. *Experiments in Fluids*, **50**, 189–200 (2011)

[12] VANIERSCHOT, M., VAN DYCK, K., SAS, P., and VAN DEN BULCK, E. Symmetry breaking and vortex precession in low-swirling annular jets. *Physics of Fluids*, **26**(10), 105110 (2014)

[13] DEL TAGLIA, C., MOSER, A., and BLUM, L. Spontaneous break of symmetry in unconfined laminar annular jets. *Journal of Fluids Engineering*, **131**(8), 081202 (2009)

[14] OGUS, G., BAELMANS, M., and VANIERSCHOT, M. On the flow structures and hysteresis of laminar swirling jets. *Physics of Fluids*, **28**(12), 123604 (2016)

[15] VANIERSCHOT, M. The break of symmetry in annular sudden expansion flows. 8*th International Symposium on Bifurcations and Instabilities in Fluid Dynamics* (*BIFD*), Limerick (2019)

[16] VANIERSCHOT, M., PERCIN, M., and VAN OUDHEUSDEN, B. W. Asymmetric vortex shedding in the wake of an abruptly expanding annular jet. *Experiments in Fluids*, **62**, 77 (2021)

[17] GRANDEMANGE, M., GOHLKE, M., and CADOT, O. Bi-stability in the turbulent wake past parallelepiped bodies with various aspect ratios and wall effects. *Physics of Fluids*, **25**(9), 095103 (2013)

[18] PAVIA, G., VARNEY, M., PASSMORE, M., and ALMOND, M. Three dimensional structure of the unsteady wake of an axisymmetric body. *Physics of Fluids*, **31**(2), 025113 (2019)

[19] KIM, W. W. and MENON, S. A new dynamic one-equation subgrid-scale model for large eddy simulations. 33*rd Aerospace Sciences Meeting and Exhibit*, American Institute of Aeronautics and Astronautics, Reno (1995)

[20] KIM, W. W. and MENON, S. An unsteady incompressible Navier-Stokes solver for large eddy simulation of turbulent flows. *International Journal for Numerical Methods in Fluids*, **31**(6), 983–1017 (1999)

[21] ZHANG, Y. and VANIERSCHOT, M. Determination of single and double helical structures in a swirling jet by spectral proper orthogonal decomposition. *Physics of Fluids*, **33**(1), 015115 (2021)

[22] BERKOOZ, G., HOLMES, P., and LUMLEY, J. L. The proper orthogonal decomposition in the analysis of turbulent flows. *Annual Review of Fluid Mechanics*, **25**(1), 539–575 (1993)

[23] SIROVICH, L. Turbulence and the dynamics of coherent structures. *Quarterly of Applied Mathematics*, **45**(3), 561–571 (1987)

[24] ZHANG, C., WAN, Z., and SUN, D. Model reduction for supersonic cavity flow using proper orthogonal decomposition (POD) and Galerkin projection. *Applied Mathematics and Mechanics* (*English Edition*), **38**(5), 723–736 (2017) https://doi.org/10.1007/s10483-017-2195-9

[25] VANIERSCHOT, M., VAN DYCK, K., and VAN DEN BULCK, E. A comparison of large scale extraction methods in the study of annular wake flow. *Flow, Turbulence and Combustion*, **91**(1), 63–77 (2013)